14th International Symposium on Turbulence and Shear Flow Phenomena (TSFP14)
Heidelberg, Germany, July 28–31, 2026

SPECTRAL PROPER ORTHOGONAL DECOMPOSITION OF THE FLOW AROUND TWO SURFACE-MOUNTED CUBES IN TANDEM

Barbara L. da Silva
Department of Mechanical and Materials Engineering
Queen's University
130 Stuart St, Kingston, Ontario,
K7L 3N6, Canada
barbara.dasilva@queensu.ca

David Sumner
Department of Mechanical Engineering
University of Saskatchewan
57 Campus Drive, Saskatoon, Saskatchewan,
S7N 5A9, Canada
david.sumner@usask.ca

Donald J. Bergstrom
Department of Mechanical Engineering
University of Saskatchewan
57 Campus Drive, Saskatoon, Saskatchewan,
S7N 5A9, Canada
don.bergstrom@usask.ca

ABSTRACT

The flow dynamics around two surface-mounted cubes in tandem were investigated for Re $= 1 \times 10^4$, $\delta/D = 0.8$ and $L/D = 2$, 2.5 and 4, representing the intermittent reattachment, cavity-locked and synchronized shedding regimes, respectively. The primary objective of the study was to identify coherent vortex shedding and wake interaction mechanisms in each regime, as well as other relevant large-scale flow modes. A spectral proper orthogonal decomposition (SPOD) was used to extract the most energetic antisymmetric and symmetric modes for each spacing ratio, based on large-eddy simulation results. Dominant antisymmetric flow modes were found to be consistent with the expected flow regime for each case. For $L/D = 2$, two dominant mode pairs represented the high- and low-frequency shedding modes from the downstream and upstream cubes, respectively. The two modes occurred independently, without bistable behaviour. A transition state was found for $L/D = 2.5$, while well-developed vortex shedding from both cubes was captured in the dominant mode for $L/D = 4$. The vortices shed from the upstream cube resembled those in the wake of an isolated cube, in contrast to vortices shed from the downstream cube, characterized by reversed streamwise vorticity signs. A low-frequency symmetric drift mode was identified for all cases, with two modes for $L/D = 4$. It was found to trigger high-frequency shedding for $L/D = 2$.

INTRODUCTION

The flow around two surface-mounted finite-height square prisms in tandem is relevant to engineering applications such as the flow around building clusters in an urban environment, the thermal management of electronic components, or momentum transfer through roughness elements. The three-dimensionality introduced by the surface-mounted and free ends of the prism, combined with wake interference effects from the tandem arrangement, leads to distinct flow regimes depending on the prisms' aspect ratio AR $= H/D$ (where H is the prism height and D is its width), the flow Reynolds number Re $= U_\infty D/\nu$ (where U_∞ is the freestream velocity and ν is the kinematic viscosity), the ground plane boundary layer thickness δ/D and the spacing ratio L/D (where L is the center-to-center longitudinal spacing between the prisms).

The flow around two surface-mounted finite prisms in tandem has been studied to evaluate sheltering effects for cylinders of different AR (Essel *et al.*, 2023), vortex generator and vortex breaker modes for square prisms with AR = 2 (Martínez-Sánchez *et al.*, 2023), and wake interference effects on turbulence anisotropy maps and the turbulence kinetic energy budget (Khan & Saha, 2021; Atzori *et al.*, 2023; Khan & Saha, 2023; Zampino *et al.*, 2025). In many of these studies, flow decomposition methods such as the proper orthogonal decomposition (POD) and dynamic mode decomposition (DMD) have been used to explore dominant interference mechanisms; moreover, the flow around two finite prisms in tandem provides a rich benchmark case for the development of new flow decomposition methods (Yuan *et al.*, 2025).

For the particular case of the flow around two surface-mounted cubes (AR = 1) in tandem, the flow can be classified in different ways depending on the analysis approach. Atzori *et al.* (2023) and Zampino *et al.* (2025) have used the broad "skimming flow", "wake interference" and "isolated roughness" designations based on mean flow field behavior. However, flow regimes can also be summarized based on the characteristics of the vortex shedding frequency, resulting in the unsynchronized shedding or intermittent reattachment regime (US, $L/D \lesssim 2.5$), cavity-locked regime (CL, $2.5 \lesssim L/D \lesssim 3.3$), and synchronized shedding regime (SS, $L/D \gtrsim 3.3$) (Havel *et al.*, 2001; Martinuzzi & Havel, 2004; da Silva *et al.*, 2024*b*). The latter classification will be adopted in the present study.

The mean flow field has been studied in detail for each of these regimes (da Silva *et al.*, 2025), but further investigation is required to verify the flow dynamics around the cubes and the mechanisms governing the development of each regime.

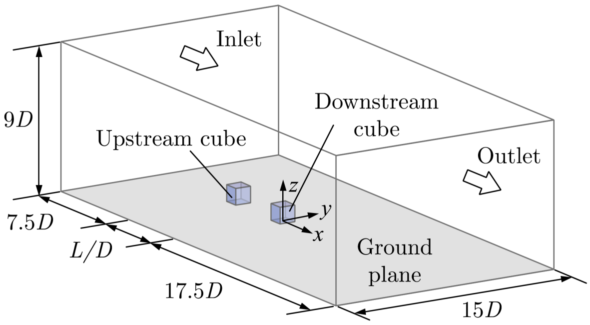

Figure 1. Schematic of the computational domain.

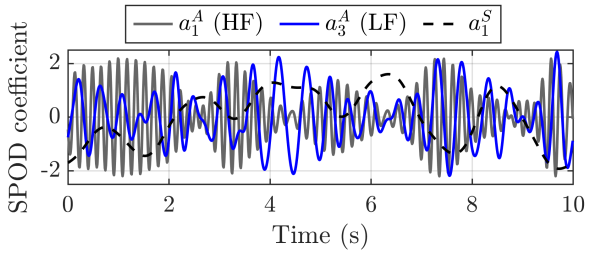

Figure 2. Time history of select SPOD mode coefficients for $L/D = 2$.

Of particular interest is the US regime, which has been found to present a bistable behaviour for two infinite square prisms in tandem (Zhou *et al.*, 2024). The present study aims to elucidate the large-scale flow dynamics in these regimes by using the SPOD. The flow around two surface-mounted cubes in tandem with $L/D = 2$ (US), 2.5 (CL) and 4 (SS) partially immersed in a turbulent boundary layer is considered, based on large-eddy simulations (LES) of the flow for $\mathrm{Re} = 1 \times 10^4$ and $\delta/D = 0.8$.

COMPUTATIONAL SET-UP

Large-eddy simulations of the flow around two surface-mounted cubes in tandem with $L/D = 2$, 2.5 and 4 were carried out using OpenFOAM 7. The computational set-up is described in detail in da Silva *et al.* (2025), but essential features are here included for completeness. The computational domain extends $25D + L$ in the streamwise (x) direction, $15D$ in the transverse (y) direction and $9D$ in the vertical (z) direction, where $D = 0.06$ m is the width of the cubes. The origin is at the center of the junction of the downstream cube with the ground plane, as shown in Fig. 1.

The domain was discretized into 10 to 11 million hexahedral elements, depending on L/D. No-slip conditions were specified on the cubes and on the ground plane, and free slip conditions were set on the top and side boundaries of the domain. The outlet had a convective outflow condition, and turbulent boundary layer data from a precursor channel flow simulation were mapped onto the bottom section of the inlet to lead to the development of a turbulent boundary layer on the ground plane. The top section of the inlet had a uniform prescribed velocity of $U_\infty = 2.5$ m/s, which led to $\mathrm{Re} = 1 \times 10^4$ and a boundary layer thickness of $\delta/D = 0.8$ at the location of the upstream cube. The $\delta/D = 0.8$ condition was chosen specifically to enable comparisons with experimental data (da Silva *et al.*, 2024*b*).

The LES was performed using the dynamic Lagrangian subgrid-scale model of Meneveau *et al.* (1996), and the conservation equations were solved using the PISO algorithm. Second-order accurate schemes were used for all terms except the advective terms of the transport equations of the integral functions of the dynamic Lagrangian subgrid-scale model, which were discretized with a first-order upwind scheme. For time advancement, the maximum Courant-Friedrichs-Lewy was maintained at approximately 1.

After a quasi-steady flow was achieved, the velocity field was sampled at a rate of 100 Hz in a uniformly distributed point cloud with a spatial resolution of $0.05D$ for a duration of 10 s (14 to 15 flow-through units). Sampled velocity fields were decomposed into symmetric and antisymmetric components, prior to decomposition with the finite-impulse response (FIR) filter-based SPOD algorithm of Sieber *et al.* (2016). A filter length of six dominant shedding periods was selected based on a sensitivity analysis to enable adequate spectral separation of the main modes, without excessive dilution of modes' energy. A feature of the FIR-based SPOD is the identification of harmonic mode pairs, based on their harmonic correlation. Results will be presented separately for the most energetic antisymmetric and symmetric mode pairs.

The mean flow field in the wake of the cubes has shown good agreement with particle image velocimetry (PIV) measurements, as shown in da Silva *et al.* (2025).

RESULTS AND DISCUSSION

Previous analyses (da Silva *et al.*, 2025) revealed that the CL ($L/D = 2.5$) and SS ($L/D = 4$) regimes are characterized by a single dominant frequency of $fD/U_\infty = 0.07$ and 0.09, respectively (where f is the frequency). On the other hand, two frequencies were identified for $L/D = 2$, of $fD/U_\infty = 0.13$ and 0.05, which is consistent with the development of the US regime. This behavior has been found in experimental studies, with different dimensionless frequency values depending on Re and boundary layer characteristics (Havel *et al.*, 2001; da Silva *et al.*, 2024*b*), yet with a similar ratio of 2–2.5 between these frequencies. The dynamics related to the dominant frequencies are captured by the most energetic antisymmetric mode pairs in each case.

Antisymmetric Modes

For $L/D = 2$, the two most energetic SPOD mode pairs account for 2.5% of the total turbulent kinetic energy. The high frequency (HF) mode ($fD/U_\infty = 0.13$) was captured by the first pair, while the second most energetic pair captured the low frequency (LF) mode ($fD/U_\infty = 0.05$). The time history of the temporal coefficients of the first antisymmetric SPOD mode, a_1^A, and the third antisymmetric mode, a_3^A, is shown in Fig. 2. The coefficients a_2 and a_4 are similar to the respective illustrated modes, but with a phase difference of $\pi/2$, since modes 1 and 2, as well as modes 3 and 4, are coupled. Figure 2 reveals that there are intervals where both SPOD modes are simultaneously weak or strong, confirming the existence of unsynchronized shedding, rather than a bistable behaviour, for $L/D = 2$. In other words, each coefficient does not consistently show high amplitude for a set period of time to the detriment of the other coefficient, which would be expected in a traditional bistable regime.

To aid in the interpretation of the flow physics related to each mode, the flow field was reconstructed with either the HF or the LF modes at four sequential instants in Fig. 3a and b, respectively. The instants cover approximately half of the

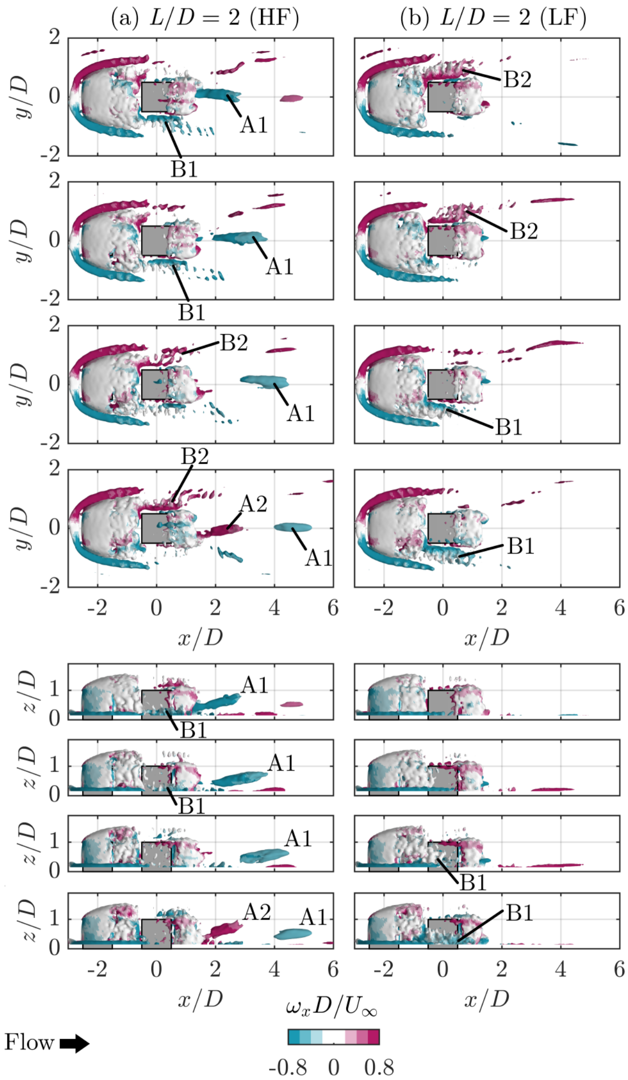

Figure 3. Isosurfaces of $QD^2/U_\infty^2 = 0.08$ colored by the streamwise vorticity $\omega_x D/U_\infty$ for the flow reconstructed with dominant antisymmetric mode pairs. Four instants and x-y and x-z views are presented. (a) HF mode pair, and (b) LF mode pair for $L/D = 2$.

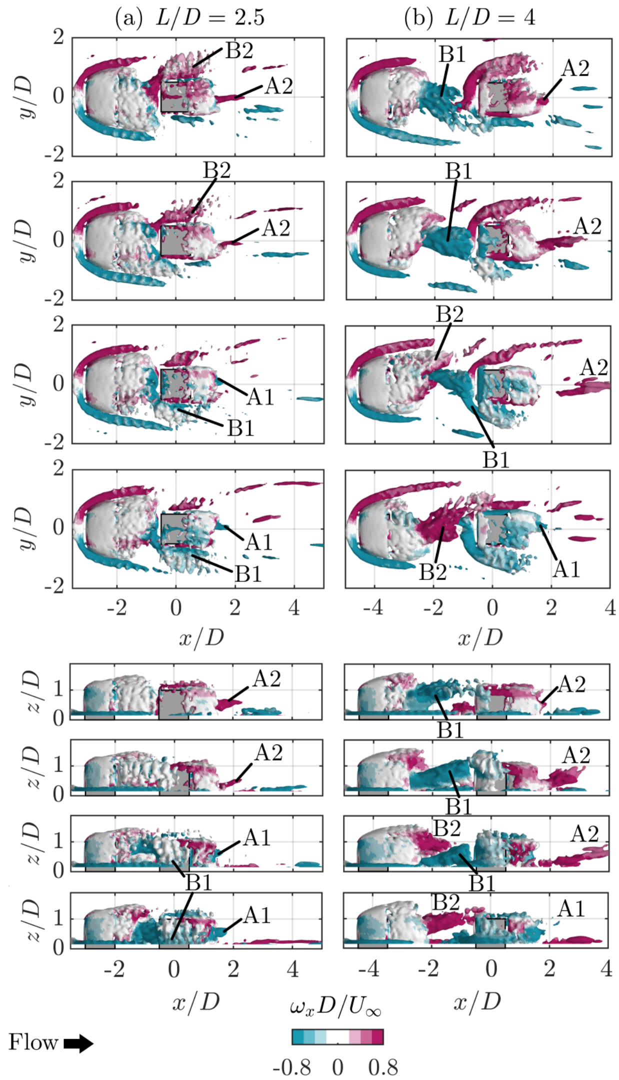

Figure 4. Isosurfaces of $QD^2/U_\infty^2 = 0.08$ colored by the streamwise vorticity $\omega_x D/U_\infty$ for the flow reconstructed with dominant antisymmetric mode pairs. Four instants and x-y and x-z views are presented. (a) $L/D = 2.5$, (b) $L/D = 4$.

corresponding period. Isosurfaces of the second invariant of the velocity gradient tensor $QD^2/U_\infty^2 = 0.08$, colored by the streamwise vorticity $\omega_x D/U_\infty$, are shown to identify the large-scale flow structures. Views from the top and from the side are included.

The HF mode for $L/D = 2$ (Fig. 3a) reveals the alternate shedding of flow structures mainly from the downstream cube. These structures are elongated in the streamwise direction, and are characterized by significant streamwise vorticity. A clockwise (blue) structure A1 is formed and shed mostly on the $+y$ side of the wake, while the counter-clockwise (pink) structure A2 is formed on the $-y$ side. Less-defined structures are found to be partially shed from the upstream cube at this frequency. Structures formed from the flow separated from the upstream cube are identified as B1 and B2 in Fig. 3, for all cases.

In the LF mode (Fig. 3b), no coherent structures are convected into the central part of the wake of the downstream cube. Large structures B1 and B2 are instead found to be released from the upstream cube's arch vortex, appearing as a stronger version of B1 and B2 in the HF mode. Even so, the weak shedding suggests that the shear layers separated from the upstream cube are not able to properly roll-up into vortices due to the presence of the downstream cube.

For $L/D = 2.5$ and the CL regime, the single most energetic SPOD antisymmetric mode pair accounts for 2.3% of the total turbulent kinetic energy and is characterized by a frequency of $fD/U_\infty = 0.07$. The flow reconstructed with this mode is presented in Fig. 4a, which reveals that structures are shed from both the downstream cube (A1/A2) and upstream cube (B1/B2). The increased gap region permits B1 and B2 to develop further before impinging on the downstream cube, yet their formation region is stretched due to the cavity-locked effect. The structures A1 and A2 are weaker than in the HF mode for $L/D = 2$, losing their coherence soon after formation. Consequently, the reconstructed flow resembles the LF mode, and this regime represents a transitional state before vortex shedding synchronization occurs for larger L/D.

The most energetic antisymmetric mode pair identified for $L/D = 4$ contributes 7.3% of the total turbulent kinetic energy. The higher energy contribution (in comparison with $L/D = 2$ and 2.5) is consistent with the SS regime. Vortex shedding from both cubes is clearly observed for the flow reconstructed with this mode, in Fig. 4b. Structures A1/A2 and B1/B2 are

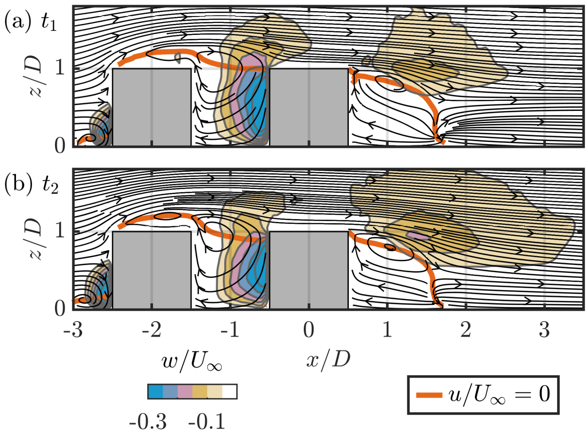

Figure 5. Reconstructed flow field for $L/D = 2$ and the symmetric drift mode at instants t_1 and t_2 that illustrate extremes of this mode. Contours of $w/U_\infty < 0$ and streamlines of the in-plane velocity field are shown in the x-z symmetry plane with $y/D = 0$.

shed with the same frequency of $fD/U_\infty = 0.09$, in agreement with experimental data (da Silva *et al.*, 2024*b*). The shape and orientation of B1 and B2 resemble those of structures shed in the wake of an isolated cube, while the A1 and A2 structures are similar to the HF mode for $L/D = 2$. The progression in Fig. 4b shows that B1 combines with and enhances the horseshoe vortex that is now formed around the downstream cube, after impinging on its front face.

While structures B1 and B2 follow the same shedding mechanism as for an isolated cube, structures A1 and A2 have distinct characteristics which indicate a different formation process. Their opposite vorticity signs in comparison with the upstream cube's vortices (on a given y side of the wake) and upward-inclined shape are compatible with the base vortices or connector strands found in quadrupole-type wakes of taller surface-mounted finite-height square prisms, suggesting a similar formation mechanism.

Symmetric Modes

The main symmetric SPOD mode pair described a low-frequency drift or shift behavior of the flow around the cubes in tandem for all L/D investigated. Also described as a pumping motion for taller surface-mounted finite-height square prisms in tandem (Essel *et al.*, 2023; Ouedraogo & Essel, 2023), this mode corresponds to a slow variation in the reverse flow area behind each prism (Essel *et al.*, 2021) and is related to the strength of the downwash of the separated flow (da Silva *et al.*, 2024*a*).

For $L/D = 2$, the drift mode was characterized by a dimensionless frequency of $fD/U_\infty = 0.01$ and contributed 0.9% of the total turbulent kinetic energy. To illustrate its dynamics, the flow was reconstructed with this mode at two instants that correspond to extremes in the temporal coefficient of the first SPOD symmetric mode, a_1^S. Figure 5 presents flooded contours of the vertical velocity component w/U_∞ in the x-z symmetry plane at these instants. Only negative values of w/U_∞ are shown for clarity, together with contours of $u/U_\infty = 0$ to indicate the reverse flow region.

Figure 5 shows a slight expansion of the reverse flow region in the gap at t_1 and its contraction at t_2, which agrees with the pumping motion observed by Ouedraogo & Essel (2023) for two finite cylinders in tandem with higher and different

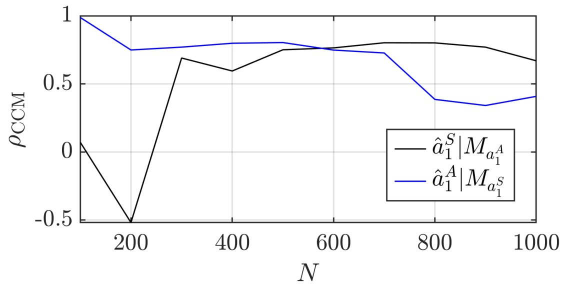

Figure 6. Correlation coefficient of the cross-map-estimated and observed SPOD coefficients a_1^S and a_1^A for $L/D = 2$.

aspect ratios. As the wake of the upstream cube contracts, the flow changes from reattachment on top of the downstream cube (Fig. 5a) to impingement on its front face (Fig. 5b). Although the reverse flow region behind the downstream cube does not change significantly throughout the drift mode, the intensity of the downwash increases at t_2, when the flow impinges on the cube's front face.

The SPOD coefficients of the drift mode for $L/D = 2$ (included in Fig. 2) show an interesting relationship with the coefficients of the antisymmetric high frequency mode, suggesting that the drift mode could be a trigger for the dominance of either the HF or LF shedding modes for $L/D = 2$. Despite the inherent limitations of the linear decomposition offered by SPOD, an assessment of the causal relationship between a_1^S and a_1^A was attempted using convergent cross mapping (CCM) (Sugihara *et al.*, 2012). The technique establishes two conditions for a causal relationship to be possible: (1) a_1^S should be able to be cross-mapped using the shadow attractor manifold of a_1^A, $M_{a_1^A}$, and (2) convergence should be observed as the number of snapshots N increases.

Figure 6 shows the correlation coefficient ρ_{CCM} between the original and cross-map-estimated variables (denoted with a hat). While a high correlation coefficient for a_1^A estimated from $M_{a_1^S}$ ($\hat{a}_1^A|M_{a_1^S}$) is observed for small values of N, convergence is not obtained, indicating that a_1^A does not cause a_1^S. In contrast, a converging behavior is observed for $\hat{a}_1^S|M_{a_1^A}$, with $\rho_{\mathrm{CCM}} = 0.67$ for $N = 1000$, suggesting a causal relationship, i.e., a_1^S influences a_1^A.

Therefore, the drift mode may be responsible for the occurrence of mode A for $L/D = 2$. This relationship indicates that, when the flow separated from the upstream cube reattaches on the downstream cube following the drift mode (Fig. 5a), the intensity of mode A and vortex shedding from the downstream cube are suppressed. In contrast, when the flow impinges on the downstream cube (Fig. 5b), the downwash in its wake becomes stronger, enabling the high-frequency vortex shedding associated with mode A.

The low-frequency drift mode for $L/D = 2.5$ shows similar features and turbulent kinetic energy contribution to the one for $L/D = 2$, but with a characteristic frequency $fD/U_\infty = 0.02$. Its isolated contribution to the flow field is shown in Fig. 7, which illustrates the reconstructed flow following the same presentation as for $L/D = 2$.

The effects of the drift mode on the reverse flow region behind the upstream cube are more pronounced for $L/D = 2.5$, causing the vertical location of flow impingement on the front face of the downstream cube to shift. A lower position of the impingement point (Fig. 7a) is accompanied by a stronger downwash in the wake of the downstream cube (more similar to $L/D = 4$), while an impingement point closer to the top

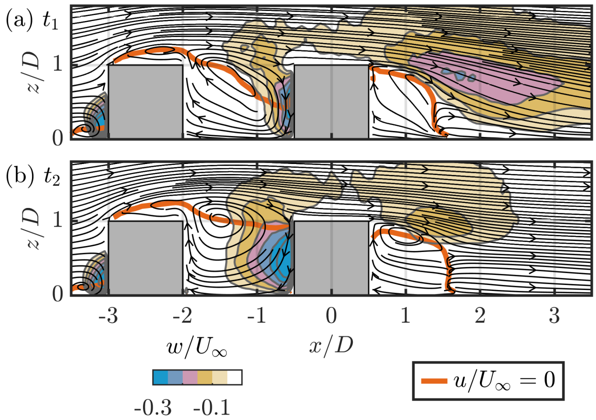

Figure 7. Reconstructed flow field for $L/D = 2.5$ and the symmetric drift mode at instants t_1 and t_2 that illustrate extremes of this mode. Contours of $w/U_\infty < 0$ and streamlines of the in-plane velocity field are shown in the x-z symmetry plane with $y/D = 0$.

edge (Fig. 7b) sees a decrease in the downwash intensity (more similar to $L/D = 2$).

Remarkably, the flow decomposition for $L/D = 4$ yielded two symmetric mode pairs which showed characteristics of drift modes. The first (most energetic) pair had peak energy at $fD/U_\infty = 0.02$ and contributed 1.1% of the total turbulent kinetic energy, while the second pair featured $fD/U_\infty = 0.01$ and a contribution of 0.9%. The flow reconstructed with each mode pair is presented in Fig. 8, showing the downward velocity component distribution and the reverse flow region in the x-z symmetry plane at extreme instants of the modes.

The first drift mode (Fig. 8a and b) features an in-phase synchronized motion between the reverse flow areas of the upstream and downstream cubes, which agrees with the pumping motion observed by Ouedraogo & Essel (2023) for two finite cylinders in tandem. This motion is accompanied by stronger downwash when the reverse flow regions have contracted (Fig. 8a), which agrees with the behavior of the drift mode in the wake of an isolated cube (da Silva *et al.*, 2024*a*).

The second drift mode (Fig. 8c and d) stands apart from the first one by showing an out-of-phase synchronization between the reverse flow regions of the upstream and downstream cube. Furthermore, the wake of the upstream cube under this mode contradicts the previously observed relationship between the downwash and the reverse flow region, with a longer wake showing correlation with stronger downwash.

CONCLUSION AND FUTURE RESULTS

Dominant large-scale shedding modes were investigated based on a SPOD of the flow around two surface-mounted cubes in tandem for $\mathrm{Re} = 1 \times 10^4$, $\delta/D = 0.8$ and $L/D = 2$, 2.5 and 4.

For $L/D = 2$, the development of unsychronized shedding was confirmed. The low and high frequencies in the wake were found to correspond to shedding from the upstream and downstream cubes, respectively. A causal analysis suggested that the low-frequency shedding mode was the nominal shedding mode of the wake, while the high-frequency mode was triggered by the low-frequency symmetric drift or shift mode for $L/D = 2$. However, it must be noted that the SPOD has inherent limitations in capturing non-linear dynamics, and further consideration should be given to the causal relationship between the drift and unsynchronized shedding modes.

The flow showed a single dominant antisymmetric mode for $L/D = 2.5$, but with weaker shedding and a symmetric drift mode that strongly related to the size of the reverse flow region in the gap. Stronger alternate shedding was observed for the synchronized shedding regime at $L/D = 4$. Vortices shed from the downstream cube featured a strong streamwise vorticity component, but differed in shape and formation mechanism from those shed by the upstream (or isolated) cube. Furthermore, the flow for $L/D = 4$ showed two drift mode pairs that described in-phase and out-of-phase changes in the extent of the reverse flow regions behind the cubes.

Acknowledgements

This study has received financial support from the National Sciences and Engineering Research Council of Canada (Discovery Grants Program numbers RGPIN 2022-04981 and 2024-03962) and the University of Saskatchewan's Dean's Scholarship program. Computational resources on the Plato cluster from Research Computing at the University of Saskatchewan and from the Digital Research Alliance of Canada are also gratefully acknowledged.

REFERENCES

Atzori, Marco, Torres, Pablo, Vidal, Alvaro, Le Clainche, Soledad, Hoyas, Sergio & Vinuesa, Ricardo 2023 High-resolution simulations of a turbulent boundary layer impacting two obstacles in tandem. *Phys. Rev. Fluids* **8** (6), 063801.

Essel, Ebenezer E., Balachandar, Ram & Tachie, Mark F. 2023 Effects of sheltering on the unsteady wake dynamics of tandem cylinders mounted in a turbulent boundary layer. *J. Fluid Mech.* **954**, A40.

Essel, Ebenezer E., Tachie, Mark F. & Balachandar, Ram 2021 Time-resolved wake dynamics of finite wall-mounted circular cylinders submerged in a turbulent boundary layer. *J. Fluid Mech.* **917**, A8.

Havel, B., Hangan, H. & Martinuzzi, R. 2001 Buffeting for 2D and 3D sharp-edged bluff bodies. *J. Wind Eng. Ind. Aerodyn.* **89** (14-15), 1369–1381.

Khan, Basheer A. & Saha, Arun K. 2021 Direct numerical simulation of turbulent flow and heat transfer over a heated cube placed in a matrix of unheated cubes. *Int. J. Heat Mass Transf.* **171**, 121052.

Khan, Basheer A. & Saha, Arun K. 2023 Effect of cube spacings on the three-dimensional flow structure over an array of wall-mounted cube. *Phys. Fluids* **35** (5), 055111.

Martinuzzi, Robert J. & Havel, Brian 2004 Vortex shedding from two surface-mounted cubes in tandem. *Int. J. Heat Fluid Flow* **25** (3), 364–372.

Martínez-Sánchez, Alvaro, Lazpita, Eneko, Corrochano, Adrián, Le Clainche, Soledad, Hoyas, Sergio & Vinuesa, Ricardo 2023 Data-driven assessment of arch vortices in simplified urban flows. *Int. J. Heat Fluid Flow* **100**, 109101.

Meneveau, Charles, Lund, Thomas S. & Cabot, William H. 1996 A Lagrangian dynamic subgrid-scale model of turbulence. *J. Fluid Mech.* **319**, 353–385.

Ouedraogo, Newton F. & Essel, Ebenezer E. 2023 Unsteady wake interference of unequal-height tandem cylinders mounted in a turbulent boundary layer. *J. Fluid Mech.* **977**, A52.

Sieber, Moritz, Paschereit, C. Oliver & Oberleithner, Kilian

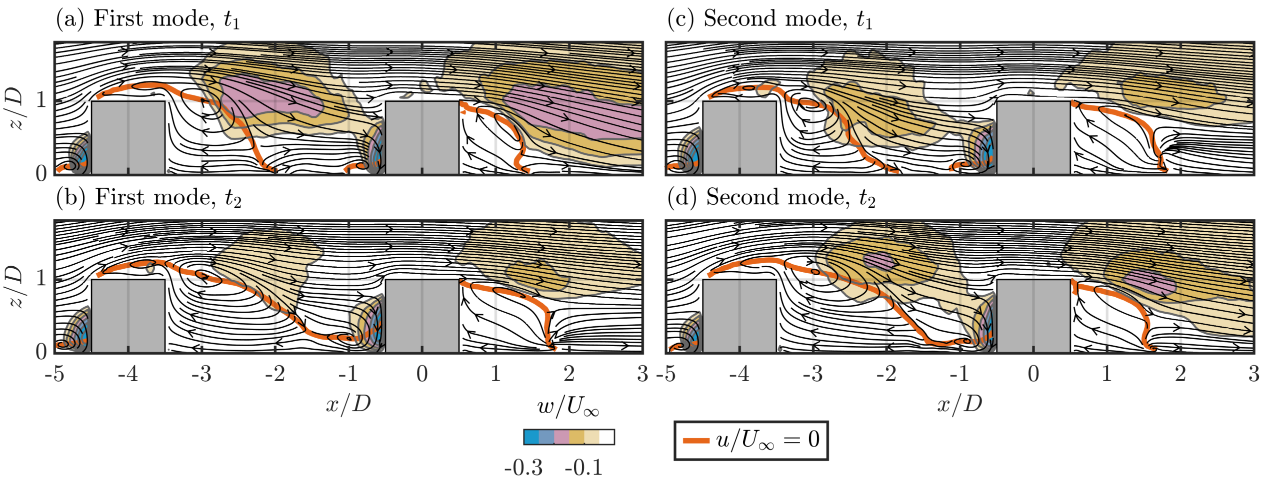

Figure 8. Reconstructed flow field for $L/D = 4$ and (a,b) the first drift mode and (c,d) the second drift mode at instants t_1 and t_2 that illustrate extremes of the modes. Contours of $w/U_\infty < 0$ and streamlines of the in-plane velocity field are shown in the x-z symmetry plane with $y/D = 0$.

2016 Spectral proper orthogonal decomposition. *J. Fluid Mech.* **792**, 798–828.

da Silva, Barbara L., Sumner, David & Bergstrom, Donald J. 2024*a* On the flow dynamics around a surface-mounted cube and boundary layer effects. *J. Fluid Mech.* **991**, A17.

da Silva, Barbara L., Sumner, David & Bergstrom, Donald J. 2024*b* Wake interference effects for two surface-mounted cubes in tandem. *Phys. Fluids* **36**, 115104.

da Silva, Barbara L., Sumner, David & Bergstrom, Donald J. 2025 Three-dimensional mean flow field around two cubes in tandem. *Int. J. Heat Fluid Flow* **116**, 109966.

Sugihara, George, May, Robert, Ye, Hao, Hsieh, Chih-Hao, Deyle, Ethan, Fogarty, Michael & Munch, Stephan 2012 Detecting causality in complex ecosystems. *Science* **338** (6106), 496–500.

Yuan, Kuiwen, Chen, Zengshun, Xu, Yemeng, Zhang, Likai, Hu, Peng & Li, Sijia 2025 Aerodynamic interference and flow field mechanisms of three-dimensional tandem square cylinders based on proper orthogonal decomposition and high-order dynamic mode decomposition modeling. *Physics of Fluids* **37** (5), 055140.

Zampino, Gerardo, Atzori, Marco & Vinuesa, Ricardo 2025 Turbulence around two obstacles in tandem: Effects of obstacle height and separation. *Phys. Fluids* **37** (7), 075171.

Zhou, Yu, Hao, Jingcheng & Alam, Md. Mahbub 2024 Wake of two tandem square cylinders. *J. Fluid Mech.* **983**, A3.